Theoretical Study of an Undisclosed Reaction Class: Direct H-Atom Abstraction from Allylic Radicals by Molecular Oxygen

Yang Li [1,*], Jin Wu [2], Qian Zhao [3], Yingjia Zhang [3] and Zuohua Huang [3]

1 Science and Technology on Combustion, Internal Flow and Thermostructure Laboratory, School of Astronautics, Northwestern Polytechnical University, Xi'an 710072, China
2 Xi'an Aerospace Propulsion Test Technology Institute, Xi'an 710100, China; lulufan0908@163.com
3 State Key Laboratory of Multiphase Flows in Power Engineering, Xi'an Jiaotong University, Xi'an 710049, China; zq950207@stu.xjtu.edu.cn (Q.Z.); yjzhang_xjtu@xjtu.edu.cn (Y.Z.); zhhuang@xjtu.edu.cn (Z.H.)
* Correspondence: yang.li@nwpu.edu.cn

Abstract: The 1-methylallyl ($C_4H_7$1-3) allylic radical is an important intermediate species in oxidation of linear C4 unsaturated hydrocarbons (1-butene, 2-butene, and 1,3-butadiene). This study reports the first high-level quantum chemical calculations for an undisclosed reaction class of this radical at intermediate to high temperatures: direct H-atom abstraction from terminal methyl group by molecular oxygen. Moreover, we systematically calculated rate constants for primary, secondary, and tertiary H-atom abstraction from the C_4, C_5, and C_6 allylic radicals, respectively. Our results can be further used as rate rules for kinetic model development of unsaturated hydrocarbon oxidation. All calculations were implemented using two different ab initio solvers: Gaussian and ORCA, three sets of ab initio methods, and two different kinetic solvers: MultiWell and PAPR. Temperature dependent rate constants and thermochemistry were carried out based on transition state theory and statistical thermodynamics, respectively. H-atom abstraction from the primary site of C4 allylic radical is found to be faster than that from secondary and tertiary sites of C5 and C6 allylic radicals, contrary to common understanding. Barrier heights predicted by different ab initio solvers and methods are about 4–5 kcal/mol different, which results in a factor of 4–86 difference in rate constant predictions depending on the temperature. Using the Gaussian solver with Method 2 is found to be the most effective combination of predicting accurate rate constants when compared against experimental data. When comparing two kinetic solvers, both reaction rate coefficients and species thermochemistry show good agreement at a wide range of temperatures, except for the rate coefficients calculated for C5 and C6 reactions (about a factor of 5–17 and 3–4 differences were obtained, respectively). From an application point of view, we incorporated the calculation results into the AramcoMech2.0 model, and found systematic improvements for predicting ignition delay time, laminar flame speed and speciation targets of 2-butene oxidation.

Keywords: allylic radicals; H-atom abstraction; quantum chemistry; rate constants; thermochemistry

1. Introduction

The combustion of hydrocarbons or oxygenates typically proceeds with H-atom abstraction by small species or radicals ($\dot{H}$, $\dot{O}H$ and O_2 etc.) from the reactant to generate a fuel radical. At high temperatures, fuel radicals may undergo H-atom abstraction by O_2 from the adjacent carbon atom to form a C = C double bond plus $H\dot{O}_2$. However, this direct abstraction reaction class: fuel radical $+O_2$ ⇄ unsaturated species $+H\dot{O}_2$ has not been found to be important; instead, fuel radicals typically undergo isomerization or β-scission reaction pathways breaking down to smaller species. This can be found in many typical and well-validated kinetic models for oxidation of alkanes [1–3], alkenes [4–8], aromatics [9–11], alcohols [12–14], aldehydes [15], ethers [16,17], and furans [18,19].

In recent mechanism development studies for 1-butene [20], 2-butene [21] and 1,3-butadiene [22] oxidation, 1-methylallyl ($C_4H_7$1-3) allylic radical was found to be the most

important intermediate species for both isomers. For 1- and 2-butene oxidation, it can be generated from allylic H-atom abstraction by hydroxyl radical (ȮH) across a wide temperature range (600–1500 K), or by molecular oxygen at high temperatures (1100–1500 K). For 1,3-butadiene oxidation, it can be produced from H-atom addition to the terminal carbon of the C = C double bond at high temperatures (1100–1500 K). At intermediate to high temperatures (900–1500 K), there are two reaction pathways for consuming this radical: (a) reactions on the $\dot{C}_4H_7$ potential energy surface (PES), and (b) direct H-atom abstraction by molecular oxygen, as shown in Figure 1.
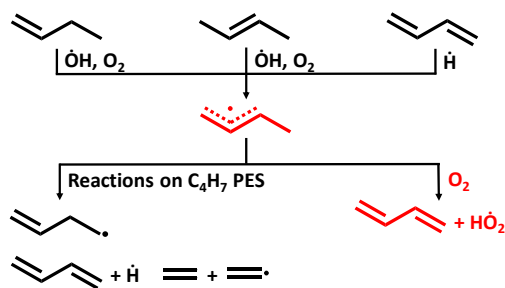

Figure 1. High temperature chemistry of 1-methylallyl ($C_4H_7$1-3) allylic radical.

For the first consumption reaction, a comprehensive theoretical study was performed to determine rate constants and thermodynamic properties of the C_4H_7 PES [23]. The scope of this study is to perform fundamental quantum chemical calculations for the second reaction route, as highlighted in red color in Figure 1. Moreover, we aim to systematically investigate rate coefficients for this reaction class, i.e., primary, secondary, and tertiary H-atom abstraction from C_4, C_5, and C_6 allylic radicals, respectively, as shown in Figure 2. Finally, rate rules will be developed for this new reaction class, which can be further used to develop kinetic models for oxidation of unsaturated hydrocarbons.
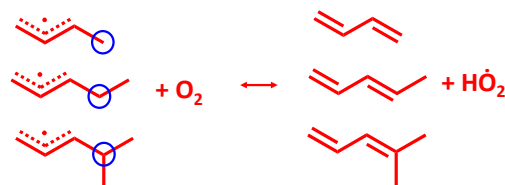

Figure 2. Reaction class for primary, secondary, and tertiary H-atom abstraction from C4, C5, and C6 allylic radicals, respectively.

We reviewed extensive publications regarding both experimental and theoretical studies of allylic radicals reacting with O_2, and these are summarized in Table S1 of Supplementary Material 1. All these studies focused on either O_2 addition reaction, or experimentally measured total rate constants. There is a lack of accurate rate coefficients for the direct H-atom abstraction reaction.

2. Computational Methods

In order to assess the accuracy of theoretical predictions, different computational methods and solvers have been employed for comparison:

- Three sets of quantum chemical methods: Method 1, Method 2, and Method 3.
- Two ab initio solvers: Gaussian 09 [24] and ORCA 4.0.0 [25].
- Two kinetic solvers: MultiWell [26] and PAPR [27].

Table 1 summarizes the three sets of quantum chemical methods adopted. They have been used effectively for rate coefficient calculations in addition, isomerization, dissociation, and abstraction reactions of C2–C9 hydrocarbons and oxygenates [22,28,29].

Table 1. Quantum chemical methods and ab initio solvers used in this study.

	Method 1	Method 2	Method 3
Ab initio solver	Gaussian and Orca		Gaussian
Geometry, frequency, scan and IRC	M06-2X/6-311++G(d,p)		
SPEs	CCSD(T)/cc-pVTZ CCSD(T)/cc-pVQZ	CCSD(T)/cc-pVDZ CCSD(T)/cc-pVTZ MP2/cc-pVDZ MP2/cc-pVTZ MP2/cc-pVQZ	G4
Zero Kelvin energies	CBS-APNO/G3/G4		

Firstly, regarding the ab initio solvers, Gaussian 09 was used for performing all three methods, while ORCA 4.0.0 was used for the calculations using Method 1 and 2. The density functional theory (DFT) method M06-2X [30] with the 6-311++G(d,p) [31,32] basis set was used for geometry optimization, vibrational frequency, dihedral angle scan, and intrinsic reaction coordinate (IRC) simultaneously in all three methods. For the electronic single-point energies (SPEs) calculation, coupled cluster theory CCSD(T)/cc-pVXZ [33] and Møller–Plesset perturbation theory MP2/cc-pVXZ [34] (where X = D, T and Q) [35] were used in Method 1 and 2, followed by complete basis set (CBS) extrapolation. While in Method 3, G4 [36] level of theory was used to calculate the SPEs directly. The T1 diagnostic [37] of all species and transition states were ≤0.030 and ≤0.036, respectively, as summarized in Table S2 in Supplementary Material 1. This indicates the reliability of single-reference methods for describing the wave function. In addition, combined compound methods CBS-APNO/G3/G4 [36,38,39] were used to calculate zero Kelvin energies (ZKEs), which were further used to derive average atomization formation enthalpies for calculation of thermodynamic properties. This method has been proved to be reliable for the thermochemistry calculation of hydrocarbons [38]. Table 2 illustrates the scale factors used for the zero-point energies (ZPEs) and vibrational frequencies, and the equations used for conducting the complete basis set (CBS) extrapolation of SPEs.

Table 2. Parameters and equations used for energy calculation in this study.

	Method 1	Method 2	Method 3
Scale factor for ZPEs	0.9698		
Scale factor for frequencies	0.983		
CBS extrapolation for SPE	$E_{CCSD(T)/cc\text{-}pVQZ} + (E_{CCSD(T)/cc\text{-}pVQZ} - E_{CCSD(T)/cc\text{-}pVTZ}) \times 4^4/(5^4 - 4^4)$	$E_{CCSD(T)/cc\text{-}pVTZ} + (E_{CCSD(T)/cc\text{-}pVTZ} - E_{CCSD(T)/cc\text{-}pVDZ}) \times 3^4/(4^4 - 3^4) + E_{MP2/cc\text{-}pVQZ} + (E_{MP2/cc\text{-}pVQZ} - E_{MP2/cc\text{-}pVTZ}) \times 4^4/(5^4 - 4^4) - E_{MP2/cc\text{-}pVTZ} + (E_{MP2/cc\text{-}pVTZ} - E_{MP2/cc\text{-}pVDZ}) \times 3^4/(4^4 - 3^4)$	E_{G4}

In both kinetic solvers, quantum mechanical tunneling was taken into account using an unsymmetrical Eckart barrier model [40], and 1-D hindered internal rotation was treated for lower frequency modes. Rate constants and thermochemistry were carried out based on canonical transition state theory (TST) [41] and statistical thermodynamics, respectively.

The calculated rate coefficients were fitted to a modified Arrhenius expression as a function of temperature:

$$k = A\left(T/T_{ref}\right)^n exp(-E/RT) \tag{1}$$

where A is the frequency factor, T is the temperature in Kelvin, $T_{ref} = 1$ K, n is the temperature exponent at 1 K, and E is related to the activation energy (by $E_a = E + nRT$).

The thermochemical properties (enthalpy of formation, entropy, and heat capacity) were calculated as a function of temperature (298.15–2000 K), and are fitted to NASA polynomials [42] using the Fitdat utility in ANSYS CHEMKIN-PRO [43].

Notably, the above methods have also been employed and explained in our recent publication [44].

3. Results and Discussion

3.1. Potential Energy Surface for $C_4H_7$1-3 + O_2 Reaction

Figure 3 shows the potential energy surface (PES) for $C_4H_7$1-3 + O_2 reaction. These two reactants can undergo: a) direct H-atom abstraction to form 1,3-butadiene (C_4H_6) plus hydroperoxy ($H\dot{O}_2$) radical and b) a barrier-less addition pathway forming an alkenyl-peroxy ($C_4H_7$1-3$\dot{O}_2$) radical, followed by $H\dot{O}_2$ concerted elimination resulting in the same products, C_4H_6 and $H\dot{O}_2$. The barrier height of the direct abstraction reaction in the first reaction pathway is 22.42 kcal/mol, and the well depth of the association reaction and the barrier height of the subsequent concerted elimination reaction in the second reaction pathway are 18.39 and 27.52 kcal/mol, respectively. Therefore, the direct abstraction pathway is kinetically favorable at intermediate to high temperatures.
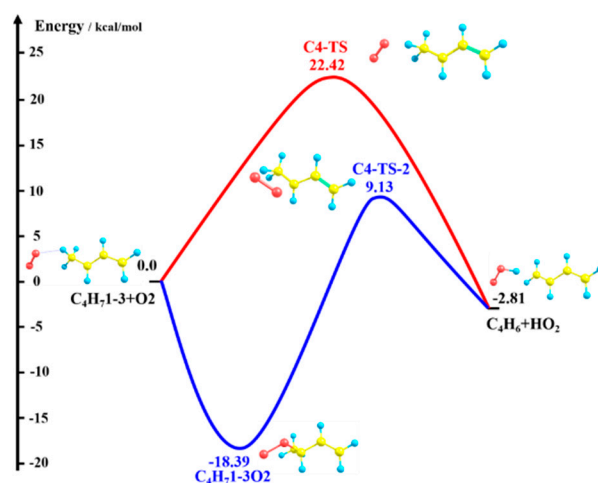

Figure 3. Potential energy surface (PES) for the $\dot{C}_4H_7$1-3 + O_2 reaction.

It is worth nothing that the two transition states (TSs) for the abstraction (C4-TS) and concerted elimination (C4-TS-2) reaction are actually connected by an internal rotation of the CC−OO dihedral angle, as shown in Figure 4. C4-TS is located at a "shallow well" with about 12 kcal/mol higher energy relative to C4-TS-2, and it is found that some DFT methods, such as wB97XD [45], tend to fail in the geometry optimization of C4-TS, and this is probably due to its "shallow well depth".

The PESs for $C_5H_9$1-3 + O_2 and C_6H_{11}1-3 + O_2 reactions have also been carried out, as shown in Figure S1 in Supplementary Material 1. Table 3 summarizes the forward and reverse barrier heights for all three abstraction reactions calculated by different methods and ab initio solvers ("-" sign means the SPE calculation was too expensive to perform). The forward barrier heights calculated by the Orca solver using Method 1 and 2 agree well with the values from the Gaussian solver using Method 3 (less than 1 kcal/mol difference). However, the results carried out by Gaussian using Method 1 and 2 are about 4-5 kcal/mol lower consistently.
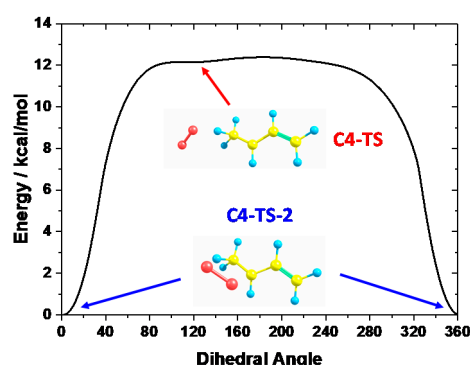
Figure 4. Internal rotor potential of the CC−OO dihedral angle for the two TSs on $C_4H_7$1-3$\dot{O}_2$ PES.

Table 3. Comparison of barrier heights. (Unit: kcal/mol).

Reactions	Method 1		Method 2		Method 3
	Orca	Gaussian	Orca	Gaussian	Gaussian
	Forward barrier height				
$C_4H_7$1-3 + $O_2 \leftrightarrow C_4H_6$ + HO_2	22.42	19.15	23.23	18.30	23.35
$C_5H_9$1-3 + $O_2 \leftrightarrow C_5H_8$ + HO_2	21.00	-	21.80	16.65	21.61
C_6H_{11}1-3 + $O_2 \leftrightarrow C_6H_{10}$ + HO_2	21.12	-	21.96	16.58	21.02
	Reverse barrier height				
$C_4H_7$1-3 + $O_2 \leftrightarrow C_4H_6$ + HO_2	25.23	22.48	26.21	22.00	25.90
$C_5H_9$1-3 + $O_2 \leftrightarrow C_5H_8$ + HO_2	27.16	-	28.09	23.63	27.06
C_6H_{11}1-3 + $O_2 \leftrightarrow C_6H_{10}$ + HO_2	28.39	-	29.31	24.58	26.94

3.2. Comparison of Rate Constants

All calculated rate constants were compared across the three different quantum chemical methods, two different ab initio solvers and two different kinetic solvers; all input and output results have been summarized in Supplementary Material 4. In this section, we pick two representatives to demonstrate the agreement or disagreement (all rate constants given are for abstraction on a per H-atom basis):

- Comparing two ab initio solvers (Gaussian and Orca) when using the MultiWell kinetic solver with Method 2
- Comparing two kinetic solvers (Multiwell and PAPR) using ab initio results from Gaussian with Method 2

Figure 5 compares the rate constants for two ab initio solvers: Orca and Gaussian. Solid and dash lines are results obtained from Gaussian and Orca solvers, respectively, and different colors correspond to three different abstraction reactions. In addition, the experimental data is plotted for the C4 reaction: $C_4H_7$1-3 + $O_2 \leftrightarrow C_4H_6$ + HO_2 measured by Knyazev et al. [46], and C5 reaction: $C_5H_9$1-3 + $O_2 \leftrightarrow C_5H_8$ + HO_2 measured by Baldwin et al. [47]. H-atom abstraction from the primary site ($C_4H_7$1-3 + O_2) was found to be faster than from secondary ($C_5H_9$1-3 + O_2) and tertiary (C_6H_{11}1-3 + O_2) sites, which seems counter-intuitive. Significant differences were found for the rate constants predicted using two ab initio solvers, being about a factor of 4–86 differences, depending on the temperature, and this is due to the difference in the barrier heights. When compared to experimental measurements, the results obtained from Gaussian solver with Method 2 show about a factor of 2 difference for both C4 and C5 reactions, which is in much better agreement with experimental data relative to the Orca solver.
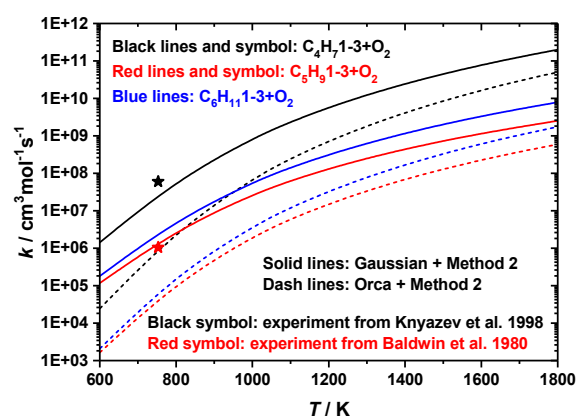
Figure 5. Rate constant comparison for two ab initio solvers: Orca and Gaussian.

Table 4 shows the rate constants comparison for two kinetic solvers: MultiWell and PAPR, over a temperature range of 600–1800 K. It is found that for the $\dot{C}_4H_7$1-3 + O_2 reaction, the two kinetic solvers show identical results, and the difference is within 10% across the entire temperature range. However, for the $C_5H_9$1-3 + O_2 and C_6H_{11}1-3 + O_2 reactions, a factor of 5–17 and 3–4 differences were obtained, respectively; the rates calculated using PAPR solver are consistently higher than those from the MultiWell solver.

Table 4. Rate constant comparison for two kinetic solvers: MultiWell and PAPR.

T/K	$C_4H_7$1-3 + O_2 Reaction		$C_5H_9$1-3 + O_2 Reaction		C_6H_{11}1-3 + O_2 Reaction	
	MultiWell	**PAPR**	**MultiWell**	**PAPR**	**MultiWell**	**PAPR**
600	1.43E + 06	1.28E + 06	1.17E + 05	5.49E + 05	1.81E + 05	5.10E + 05
800	6.37E + 07	6.12E + 07	3.01E + 06	2.04E + 07	5.58E + 06	1.74E + 07
1000	8.61E + 08	8.62E + 08	2.71E + 07	2.41E + 08	5.77E + 07	1.91E + 08
1100	2.38E + 09	2.42E + 09	6.35E + 07	6.31E + 08	1.44E + 08	4.88E + 08
1200	5.75E + 09	5.92E + 09	1.33E + 08	1.45E + 09	3.17E + 08	1.10E + 09
1300	1.24E + 10	1.30E + 10	2.52E + 08	3.02E + 09	6.35E + 08	2.24E + 09
1400	2.46E + 10	2.59E + 10	4.44E + 08	5.78E + 09	1.17E + 09	4.21E + 09
1500	4.53E + 10	4.81E + 10	7.35E + 08	1.03E + 10	2.04E + 09	7.40E + 09
1600	7.82E + 10	8.39E + 10	1.16E + 09	1.73E + 10	3.34E + 09	1.23E + 10
1700	1.28E + 11	1.39E + 11	1.74E + 09	2.78E + 10	5.25E + 09	1.96E + 10
1800	2.01E + 11	2.20E + 11	2.53E + 09	4.28E + 10	7.91E + 09	2.98E + 10

3.3. Thermodynamic Properties

In order to demonstrate the reliability of the calculated thermodynamic properties, three widely accepted thermochemistry databases were selected for comparison:

- This study: CBS-APNO/G3/G4//M06-2X/6-311++G(d,p).
- Thermochemical Data of Organic Compounds (TDOC) by Pedley et al. [48]: experiments.
- Active Thermochemical Tables (ATcT): refs. [49–51].
- Goldsmith et al. [52]: RQCISD(T)/cc-pVT,QZ//B3LYP/6-311++G(d,p), with bond additivity correction.

Table 5 compares the thermochemistry for closed shell molecules: C_4H_6, C_5H_8, and C_6H_{10}. Excellent agreement is obtained for the 298 K enthalpies of formation ($\Delta_f H^{\ominus}$), 298 K entropies ($S^{\ominus}$), and heat capacities (C_p) at selected temperatures (the difference is within 0.5 kcal mol^{-1} and 0.5 cal K^{-1} mol^{-1}).

Table 6 compares the thermodynamic properties calculated by two kinetic solvers (MultiWell and PAPR) for allylic radicals: $\dot{C}_4H_7$1-3, $\dot{C}_5H_9$1-3 and $\dot{C}_6H_{11}$1-3. The $\Delta_f H^{\ominus}$, $S^{\ominus}$ and C_p at selected temperatures calculated using MultiWell and PAPR are in excellent agreement, with less than 0.5 kcal mol^{-1} or 0.5 cal K^{-1} mol^{-1} difference of one another across the entire temperature range.

Table 5. Thermochemistry comparison of closed shell molecules. (Units: kcal mol^{-1} for $\Delta_f H^{\ominus}$, cal K^{-1} mol^{-1} for $S^{\ominus}$ and C_p.)

		$\Delta_f H^{\ominus}$	$S^{\ominus}$	C_p						
Molecules	Source	298 K	298 K	300 K	400 K	500 K	600 K	800 K	1000 K	1500 K
	This study	26.7	66.6	18.9	24.3	28.7	32.1	37.1	40.7	46.3
C_4H_6	ATcT	26.5	-	-	-	-	-	-	-	-
	TDOC	26.3	-	-	-	-	-	-	-	-
	Goldsmith et al.	26.5	65.8	18.5	24.0	28.7	32.4	37.6	41.1	46.6
C_5H_8	*This study*	18.7	76.5	24.4	30.9	36.4	41.0	47.8	52.7	60.4
	TDOC	18.2	-	-	-	-	-	-	-	-
C_6H_{10}	Current study	11.0	84.9	29.8	37.6	44.3	49.7	58.1	64.3	74.2

Table 6. Thermochemistry comparison of allylic radicals. (Units: kcal mol^{-1} for $\Delta_f H^{\ominus}$, cal K^{-1} mol^{-1} for $S^{\ominus}$ and C_p).

		$\Delta_f H^{\ominus}$	$S^{\ominus}$	C_p						
Radicals	Source	298 K	298 K	300 K	400 K	500 K	600 K	800 K	1000 K	1500 K
$C_4H_7$1-3	MultiWell	31.9	72.1	19.7	24.8	29.3	33.1	39.1	43.6	50.6
	PAPR	31.7	72.0	19.9	24.8	29.3	33.3	39.2	43.7	50.6
$C_5H_9$1-3	MultiWell	26.8	83.1	25.2	31.8	37.6	42.5	50.1	55.8	64.8
	PAPR	27.2	83.3	25.5	32.6	38.2	43.1	50.5	56.1	64.9
C_6H_{11}1-3	MultiWell	19.8	88.9	31.4	39.4	46.5	52.4	61.6	68.4	79.1
	PAPR	19.8	89.1	31.2	39.0	46.2	52.4	61.5	68.4	79.1

3.4. Application in Kinetic Model Development

One of the major applications of accurate rate constants and thermochemistry is for the development of detailed chemical kinetic models. In this section, we incorporated all rate coefficients and thermodynamic properties calculated using the combination of: (a) Gaussian solver, (b) Method 1, (c) MultiWell solver into AramcoMech 2.0 [21]. In addition, we included the other two recently published quantum calculations for two more important high-temperature oxidation reaction classes of C4 unsaturated hydrocarbons:

- Reactions on the $\dot{C}_4H_7$ PES by Li et al. [23]
- Allylic H-atom abstraction by O_2 from 1- and 2-butene by Zhou et al. [28]

Here, 2-butene was selected as a representative in the AramcoMech 2.0 model, wherein the rate constant assigned to the $\dot{C}_4H_7$1-3 + O_2 ⇌ C_4H_6 + $H\dot{O}_2$ reaction was based on analogy to the theoretical prediction of $I\dot{C}_3H_7$ + O_2 ⇌ C_3H_6 + $H\dot{O}_2$ reaction from DeSain et al. [53]. A comparison against rates calculated here is given in Figure S2 in Supplementary Material 1. Figure 6 shows the validation results for the following key targets of high-temperature oxidation:

- Ignition delay time [21]
- Laminar flame speed [54]
- Speciation in JSR [55]

In the figure, all symbols are experimental data obtained from literature, while the dash and solid lines are simulation results using the original AramcoMech 2.0 model and the model with new rate constants, respectively. The improvement of model prediction across-the-board further indicates the reliability of the above quantum calculation results. A further detailed analysis of its effects on kinetic mechanism is beyond the scope of this study and will be included in future works. Notably, the reactants' profile shown in "(c) Speciation validation" shows quite large fluctuation, and the accuracy of these data is suspicious.
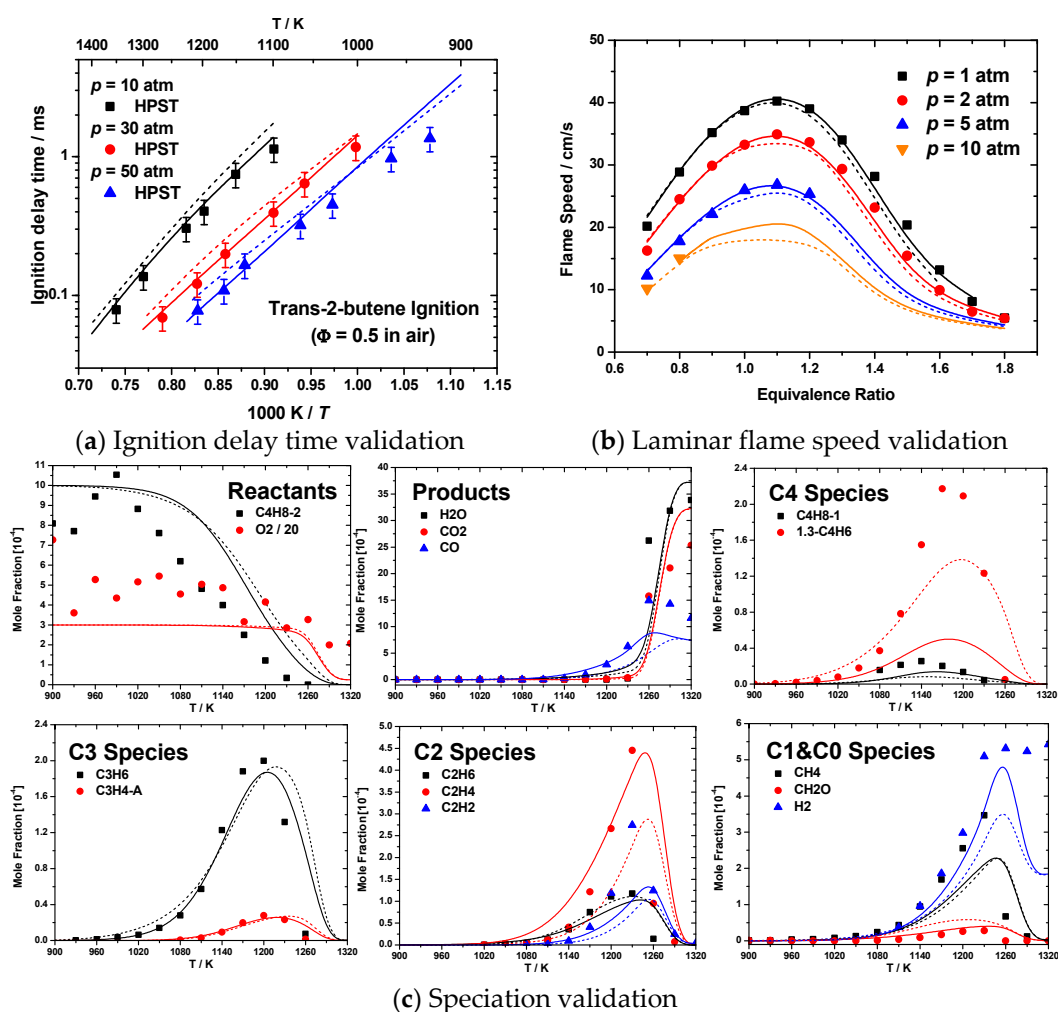
(**a**) Ignition delay time validation (**b**) Laminar flame speed validation

(**c**) Speciation validation

Figure 6. Ignition delay time, laminar flame speed, and speciation validation results for 2-butene.

4. Conclusions

This work presented comprehensive quantum chemical calculations for a new reaction class: H-atom abstraction from C4-C6 allylic radicals by molecular oxygen. The calculated potential energy surface of $\dot{C}_4H_7$1-3 + O_2 reaction showed that direct H-atom abstraction has a lower barrier height compared to that of $H\dot{O}_2$ concerted elimination, which makes the former kinetically favorable at intermediate to high temperatures. Rate constants for the three reactions and thermochemistry of species involved in each reaction were systematically calculated using two different ab initio solvers (Orca and Gaussian), three sets of ab initio methods, and two different kinetic solvers (MultiWell and PAPR). The results were compared against each other, as well as against experimental results in literature. Notably, all fitted rate coefficients and thermodynamic properties were summarized in Supplementary Material 2, and species glossary was provided in Supplementary Material 3.

It was found that the Gaussian solver plus Method 1 and 2 generally predicts lower barriers than the Orca solver plus Method 1 and 2 and the Gaussian solver plus Method 3, by about 4-5 kcal/mol consistently; this results in about a factor of 4-86 difference in rate constant predictions in the temperature range of 600–1800 K. H-atom abstraction from the primary site ($\dot{C}_4H_7$1-3 + O_2) was found to be faster than from secondary ($\dot{C}_5H_9$1-3 + O_2) and tertiary ($\dot{C}_6H_{11}$1-3 + O_2) sites, and the Gaussian solver plus Method 2 (CCSD(T)/cc-pVXZ&MP2/cc-pVXZ//M06-2X/6-311++G(d,p), where X = D, T and Q) predicts rate constants with the highest accuracy; about a factor of 2 difference compared against the experimental data. For the thermochemistry calculations, the temperature dependent

enthalpy of formation, entropy and heat capacity of closed shell molecules: C_4H_6, C_5H_8 and C_6H_{10} were compared against some well-known literature values, and excellent agreement was obtained with less than 0.5 kcal mol^{-1} difference for standard enthalpy of formation and 0.5 cal K^{-1} mol^{-1} for entropy at 298 K and heat capacity from 300–2000 K, respectively. Good agreement was also obtained for both rate coefficients and thermodynamic properties calculations using two kinetic solvers, MultiWell and PAPR, except for the rate coefficients prediction of C5 and C6 reactions (about a factor of 5–17 and 3–4 differences were obtained, respectively). Finally, we incorporated all calculated results into the AramcoMech 2.0 model, and a systematic improvement was observed in ignition delay times, laminar flame speeds, and speciation for 2-butene oxidation.

Supplementary Materials: The following are available online at https://www.mdpi.com/article/10.3390/en14102916/s1, Figure S1: title, Table S1: title, Video S1: title. Supplementary Material 1: Additional information. Supplementary Material 2: All fitted rate coefficients and thermodynamic properties. Supplementary Material 3: Species Glossary. Supplementary Material 4: All input and output files for MultiWell and PAPR solvers. References [46,47,56–69] are cited in Supplementary Material 1.

References

1. Zhang, K.; Banyon, C.; Togbé, C.; Dagaut, P.; Bugler, J.; Curran, H.J. An experimental and kinetic modeling study of n-hexane oxidation. *Combust. Flame* **2015**, *162*, 4194–4207. [CrossRef]
2. Zhang, K.; Banyon, C.; Bugler, J.; Curran, H.J.; Rodriguez, A.; Herbinet, O.; Battin-Leclerc, F.; B'Chir, C.; Heufer, K.A. An updated experimental and kinetic modeling study of n-heptane oxidation. *Combust. Flame* **2016**, *172*, 116–135. [CrossRef]
3. Atef, N.; Kukkadapu, G.; Mohamed, S.Y.; Rashidi, M.A.; Banyon, C.; Mehl, M.; Heufer, K.A.; Nasir, E.F.; Alfazazi, A.; Das, A.K.; et al. A comprehensive iso-octane combustion model with improved thermochemistry and chemical kinetics. *Combust. Flame* **2017**, *178*, 111–134. [CrossRef]
4. Kopp, M.M.; Donato, N.S.; Petersen, E.L.; Metcalfe, W.K.; Burke, S.M.; Curran, H.J. Oxidation of Ethylene–Air Mixtures at Elevated Pressures, Part 1: Experimental Results. *J. Propuls. Power* **2014**, *30*, 790–798. [CrossRef]
5. Kopp, M.M.; Petersen, E.L.; Metcalfe, W.K.; Burke, S.M.; Curran, H.J. Oxidation of Ethylene—Air Mixtures at Elevated Pressures, Part 2: Chemical Kinetics. *J. Propuls. Power* **2014**, *30*, 799–811. [CrossRef]
6. Burke, S.M.; Metcalfe, W.; Herbinet, O.; Battin-Leclerc, F.; Haas, F.M.; Santner, J.; Dryer, F.L.; Curran, H.J. An experimental and modeling study of propene oxidation. Part 1: Speciation measurements in jet-stirred and flow reactors. *Combust. Flame* **2014**, *161*, 2765–2784. [CrossRef]
7. Burke, S.M.; Burke, U.; Mc Donagh, R.; Mathieu, O.; Osorio, I.; Keesee, C.; Morones, A.; Petersen, E.L.; Wang, W.; DeVerter, T.A.; et al. An experimental and modeling study of propene oxidation. Part 2: Ignition delay time and flame speed measurements. *Combust. Flame* **2015**, *162*, 296–314. [CrossRef]
8. Zhou, C.-W.; Li, Y.; O'Connor, E.; Somers, K.P.; Thion, S.; Keesee, C.; Mathieu, O.; Petersen, E.L.; DeVerter, T.A.; Oehlschlaeger, M.A.; et al. A comprehensive experimental and modeling study of isobutene oxidation. *Combust. Flame* **2016**, *167*, 353–379. [CrossRef]
9. Zhang, Y.; Somers, K.P.; Mehl, M.; Pitz, W.J.; Cracknell, R.F.; Curran, H.J. Probing the antagonistic effect of toluene as a component in surrogate fuel models at low temperatures and high pressures. A case study of toluene/dimethyl ether mixtures. *Proc. Combust. Inst.* **2017**, *36*, 413–421. [CrossRef]

10. Yuan, W.; Li, Y.; Pengloan, G.; Togbé, C.; Dagaut, P.; Qi, F. A comprehensive experimental and kinetic modeling study of ethylbenzene combustion. *Combust. Flame* **2016**, *166*, 255–265. [CrossRef]

11. Dagaut, P.; Ristori, A.; El Bakali, A.; Cathonnet, M. Experimental and kinetic modeling study of the oxidation of n-propylbenzene. *Fuel* **2002**, *81*, 173–184. [CrossRef]

12. Zhang, Y.; El-Merhubi, H.; Lefort, B.; Le Moyne, L.; Curran, H.J.; Kéromnès, A. Probing the low-temperature chemistry of ethanol via the addition of dimethyl ether. *Combust. Flame* **2018**, *190*, 74–86. [CrossRef]

13. Frassoldati, A.; Cuoci, A.; Faravelli, T.; Niemann, U.; Ranzi, E.; Seiser, R.; Seshadri, K. An experimental and kinetic modeling study of n-propanol and iso-propanol combustion. *Combust. Flame* **2010**, *157*, 2–16. [CrossRef]

14. Sarathy, S.M.; Vranckx, S.; Yasunaga, K.; Mehl, M.; Oßwald, P.; Metcalfe, W.K.; Westbrook, C.K.; Pitz, W.J.; Kohse-Höinghaus, K.; Fernandes, R.X.; et al. A comprehensive chemical kinetic combustion model for the four butanol isomers. *Combust. Flame* **2012**, *159*, 2028–2055. [CrossRef]

15. Pelucchi, M.; Somers, K.P.; Yasunaga, K.; Burke, U.; Frassoldati, A.; Ranzi, E.; Curran, H.J.; Faravelli, T. An experimental and kinetic modeling study of the pyrolysis and oxidation of n-C3C5 aldehydes in shock tubes. *Combust. Flame* **2015**, *162*, 265–286. [CrossRef]

16. Burke, U.; Somers, K.P.; O'Toole, P.; Zinner, C.M.; Marquet, N.; Bourque, G.; Petersen, E.L.; Metcalfe, W.K.; Serinyel, Z.; Curran, H.J. An ignition delay and kinetic modeling study of methane, dimethyl ether, and their mixtures at high pressures. *Combust. Flame* **2015**, *162*, 315–330. [CrossRef]

17. Yasunaga, K.; Gillespie, F.; Simmie, J.M.; Curran, H.J.; Kuraguchi, Y.; Hoshikawa, H.; Yamane, M.; Hidaka, Y. A Multiple Shock Tube and Chemical Kinetic Modeling Study of Diethyl Ether Pyrolysis and Oxidation. *J. Phys. Chem.* **2010**, *114*, 9098–9109. [CrossRef]

18. Somers, K.P.; Simmie, J.M.; Gillespie, F.; Burke, U.; Connolly, J.; Metcalfe, W.K.; Battin-Leclerc, F.; Dirrenberger, P.; Herbinet, O.; Glaude, P.A.; et al. A high temperature and atmospheric pressure experimental and detailed chemical kinetic modelling study of 2-methyl furan oxidation. *Proc. Combust. Inst.* **2013**, *34*, 225–232. [CrossRef]

19. Somers, K.P.; Simmie, J.M.; Gillespie, F.; Conroy, C.; Black, G.; Metcalfe, W.K.; Battin-Leclerc, F.; Dirrenberger, P.; Herbinet, O.; Glaude, P.-A.; et al. A comprehensive experimental and detailed chemical kinetic modelling study of 2,5-dimethylfuran pyrolysis and oxidation. *Combust. Flame* **2013**, *160*, 2291–2318. [CrossRef]

20. Li, Y.; Zhou, C.-W.; Curran, H.J. An extensive experimental and modeling study of 1-butene oxidation. *Combust. Flame* **2017**, *181*, 198–213. [CrossRef]

21. Li, Y.; Zhou, C.-W.; Somers, K.P.; Zhang, K.; Curran, H.J. The oxidation of 2-butene: A high pressure ignition delay, kinetic modeling study and reactivity comparison with isobutene and 1-butene. *Proc. Combust. Inst.* **2017**, *36*, 403–411. [CrossRef]

22. Zhou, C.-W.; Li, Y.; Burke, U.; Banyon, C.; Somers, K.P.; Ding, S.; Khan, S.; Hargis, J.W.; Sikes, T.; Mathieu, O.; et al. An experimental and chemical kinetic modeling study of 1,3-butadiene combustion: Ignition delay time and laminar flame speed measurements. *Combust. Flame* **2018**, *197*, 423–438. [CrossRef]

23. Li, Y.; Klippenstein, S.J.; Zhou, C.-W.; Curran, H.J. Theoretical Kinetics Analysis for Ḣ Atom Addition to 1,3-Butadiene and Related Reactions on the Ċ4H7 Potential Energy Surface. *J. Phys. Chem.* **2017**, *121*, 7433–7445. [CrossRef]

24. Foresman, J.; Ortiz, J.; Cioslowski, J.; Fox, D. *Gaussian 09, Revision, D. 01*; Gaussian, Inc.: Wallingford, CT, USA, 2009.

25. Neese, F. The ORCA program system. *Wiley Interdiscip. Rev. Comput. Mol. Sci.* **2012**, *2*, 73–78. [CrossRef]

26. Barker, J.R.; Nguyen, T.L.; Stanton, J.F.; Aieta, C.; Ceotto, M.; Gabas, F.; Kumar, T.J.D.; Li, C.G.L.; Lohr, L.L.; Maranzana, A.; et al. *MultiWell-2016 Software Suite*; Barker, J.R., Ed.; University of Michigan: Ann Arbor, MI, USA, 2016.

27. Georgievskii, Y.; Miller, J.A.; Burke, M.P.; Klippenstein, S.J. Reformulation and Solution of the Master Equation for Multiple-Well Chemical Reactions. *J. Phys. Chem.* **2013**, *117*, 12146–12154. [CrossRef] [PubMed]

28. Zhou, C.-W.; Simmie, J.M.; Somers, K.P.; Goldsmith, C.F.; Curran, H.J. Chemical Kinetics of Hydrogen Atom Abstraction from Allylic Sites by $^3O_2$; Implications for Combustion Modeling and Simulation. *J. Phys. Chem.* **2017**, *121*, 1890–1899. [CrossRef] [PubMed]

29. Bugler, J.; Power, J.; Curran, H.J. A theoretical study of cyclic ether formation reactions. *Proc. Combust. Inst.* **2017**, *36*, 161–167. [CrossRef]

30. Zhao, Y.; Truhlar, D.G. The M06 suite of density functionals for main group thermochemistry, thermochemical kinetics, noncovalent interactions, excited states, and transition elements: Two new functionals and systematic testing of four M06-class functionals and 12 other functionals. *Theor. Chem. Acc.* **2008**, *120*, 215–241. [CrossRef]

31. McLean, A.D.; Chandler, G.S. Contracted Gaussian basis sets for molecular calculations. I. Second row atoms, Z = 11−18. *J. Chem. Phys.* **1980**, *72*, 5639–5648. [CrossRef]

32. Krishnan, R.; Binkley, J.S.; Seeger, R.; Pople, J.A. Self-consistent molecular orbital methods. XX. A basis set for correlated wave functions. *J. Chem. Phys.* **1980**, *72*, 650–654. [CrossRef]

33. Purvis, G.D., III; Bartlett, R.J. A full coupled-cluster singles and doubles model: The inclusion of disconnected triples. *J. Chem. Phys.* **1982**, *76*, 1910–1918. [CrossRef]

34. Møller, C.; Plesset, M.S. Note on an Approximation Treatment for Many-Electron Systems. *Phys. Rev.* **1934**, *46*, 618–622. [CrossRef]

35. Dunning, T.H., Jr. Gaussian basis sets for use in correlated molecular calculations. I. The atoms boron through neon and hydrogen. *J. Chem. Phys.* **1989**, *90*, 1007–1023. [CrossRef]

36. Curtiss, L.A.; Redfern, P.C.; Raghavachari, K. Gaussian-4 theory. *J. Chem. Phys.* **2007**, *126*, 084108. [CrossRef] [PubMed]

37. Lee, T.J.; Taylor, P.R. A diagnostic for determining the quality of single-reference electron correlation methods. *Int. J. Quantum Chem.* **1989**, *36*, 199–207. [CrossRef]

38. Ochterski, J.W.; Petersson, G.A.; Montgomery, J.A., Jr. A complete basis set model chemistry. V. Extensions to six or more heavy atoms. *J. Chem. Phys.* **1996**, *104*, 2598–2619. [CrossRef]

39. Curtiss, L.A.; Raghavachari, K.; Redfern, P.C.; Rassolov, V.; Pople, J.A. Gaussian-3 (G3) theory for molecules containing first and second-row atoms. *J. Chem. Phys.* **1998**, *109*, 7764–7776. [CrossRef]

40. Eckart, C. The Penetration of a Potential Barrier by Electrons. *Phys. Rev.* **1930**, *35*, 1303–1309. [CrossRef]

41. Eyring, H. The Activated Complex in Chemical Reactions. *J. Chem. Phys.* **1935**, *3*, 107–115. [CrossRef]

42. Gordon, S.; Mcbride, B.J. Computer Program for Calculation of Complex Chemical Equilibrium Compositions, Rocket Performance, Incident and Reflected Shocks, and Chapman-Jouguet Detonations. *Nasa Sti* **1976**, *273*, 119–224.

43. ANSYS, Inc. *ANSYS Chemkin-Pro 17.2*; ANSYS, Inc.: San Diego, CA, USA, 2016.

44. Li, Y.; Sarathy, S.M. Probing hydrogen–nitrogen chemistry: A theoretical study of important reactions in NxHy, HCN and HNCO oxidation. *Int. J. Hydrog. Energy* **2020**, *45*, 23624–23637. [CrossRef]

45. Chai, J.-D.; Head-Gordon, M. Long-range corrected hybrid density functionals with damped atom–atom dispersion corrections. *PCCP* **2008**, *10*, 6615–6620. [CrossRef] [PubMed]

46. Knyazev, V.D.; Slagle, I.R. Thermochemistry and Kinetics of the Reaction of 1-Methylallyl Radicals with Molecular Oxygen. *J. Phys. Chem.* **1998**, *102*, 8932–8940. [CrossRef]

47. Baldwin, R.R.; Bennett, J.P.; Walker, R.W. Addition of pentenes to slowly reacting mixtures of hydrogen and oxygen at 480 °C. *J. Chem. Soc. Faraday Trans. Phys. Chem. Condens. Phases* **1980**, *76*, 2396–2412. [CrossRef]

48. Pedley, J.B. *Thermochemical Data of Organic Compounds*; Springer: Dordrecht, The Netherlands, 2012.

49. Ruscic, B.; Pinzon, R.E.; Morton, M.L.; von Laszevski, G.; Bittner, S.J.; Nijsure, S.G.; Amin, K.A.; Minkoff, M.; Wagner, A.F. Introduction to Active Thermochemical Tables: Several "Key" Enthalpies of Formation Revisited. *J. Phys. Chem.* **2004**, *108*, 9979–9997. [CrossRef]

50. Branko, R.; Reinhardt, E.P.; Gregor von, L.; Deepti, K.; Alexander, B.; David, L.; David, M.; Albert, F.W. Active Thermochemical Tables: Thermochemistry for the 21st century. *J. Phys. Conf. Ser.* **2005**, *16*, 561.

51. Ruscic, B.; Feller, D.; Peterson, K.A. Active Thermochemical Tables: Dissociation energies of several homonuclear first-row diatomics and related thermochemical values. *Theor. Chem. Acc.* **2013**, *133*, 1415. [CrossRef]

52. Goldsmith, C.F.; Magoon, G.R.; Green, W.H. Database of Small Molecule Thermochemistry for Combustion. *J. Phys. Chem.* **2012**, *116*, 9033–9057. [CrossRef]

53. DeSain, J.D.; Klippenstein, S.J.; Miller, J.A.; Taatjes, C.A. Measurements, Theory, and Modeling of OH Formation in Ethyl + O$_2$ and Propyl + O$_2$ Reactions. *J. Phys. Chem.* **2003**, *107*, 4415–4427. [CrossRef]

54. Zhao, P.; Yuan, W.; Sun, H.; Li, Y.; Kelley, A.P.; Zheng, X.; Law, C.K. Laminar flame speeds, counterflow ignition, and kinetic modeling of the butene isomers. *Proc. Combust. Inst.* **2015**, *35*, 309–316. [CrossRef]

55. Fenard, Y.; Dagaut, P.; Dayma, G.; Halter, F.; Foucher, F. Experimental and kinetic modeling study of trans-2-butene oxidation in a jet-stirred reactor and a combustion bomb. *Proc. Combust. Inst.* **2015**, *35*, 317–324. [CrossRef]

56. Ruiz, R.P.; Bayes, K.D.; Macpherson, M.T.; Pilling, M.J. Direct observation of the equilibrium between allyl radicals, oxygen, and allylperoxy radicals. *J. Phys. Chem.* **1981**, *85*, 1622–1624. [CrossRef]

57. Morgan, C.A.; Pilling, M.J.; Tulloch, J.M.; Ruiz, R.P.; Bayes, K.D. Direct determination of the equilibrium constant and thermodynamic parameters for the reaction. C3H5+ O2 ⇌ C3H5O2. *J. Chem. Soc. Faraday Trans. 2 Mol. Chem. Phys.* **1982**, *78*, 1323–1330. [CrossRef]

58. Slagle, I.R.; Ratajczak, E.; Heaven, M.C.; Gutman, D.; Wagner, A.F. Kinetics of polyatomic free radicals produced by laser photolysis. 4. Study of the equilibrium isopropyl + oxygen .tautm. isopropylperoxy between 592 and 692 K. *J. Am. Chem. Soc.* **1985**, *107*, 1838–1845. [CrossRef]

59. Baldwin, R.R.; Lodhi, Z.H.; Stothard, N.; Walker, R.W. The oxidation chemistry of allyl radicals and related 'stable' radicals. *Symp. Int. Combust.* **1991**, *23*, 123–130. [CrossRef]

60. Lodhi, Z.H.; Walker, R.W. Oxidation of allyl radicals: Kinetic parameters for the reactions of allyl radicals with HO2 and O2 between 400 and 480 °C. *J. Chem. Soc. Faraday Trans.* **1991**, *87*, 2361–2365. [CrossRef]

61. Lodhi, Z.H.; Walker, R.W. Decomposition of 4,4-dimethylpent-1-ene in the presence of oxygen between 400 and 500 °C: Oxidation chemistry of allyl radicals. *J. Chem. Soc. Faraday Trans.* **1991**, *87*, 681–689. [CrossRef]

62. Stothard, N.D.; Walker, R.W. Oxidation chemistry of propene in the autoignition region: Arrhenius parameters for the allyl + O2 reaction pathways and kinetic data for initiation reactions. *J. Chem. Soc. Faraday Trans.* **1992**, *88*, 2621–2629. [CrossRef]

63. Bozzelli, J.W.; Dean, A.M. Hydrocarbon radical reactions with oxygen: Comparison of allyl, formyl, and vinyl to ethyl. *J. Phys. Chem.* **1993**, *97*, 4427–4441. [CrossRef]

64. Chen, C.-J.; Bozzelli, J.W. Thermochemical Property, Pathway and Kinetic Analysis on the Reactions of Allylic Isobutenyl Radical with O2: an Elementary Reaction Mechanism for Isobutene Oxidation. *J. Phys. Chem. A* **2000**, *104*, 9715–9732. [CrossRef]

65. Pratt, D.A.; Mills, J.H.; Porter, N.A. Theoretical Calculations of Carbon−Oxygen Bond Dissociation Enthalpies of Peroxyl Radicals Formed in the Autoxidation of Lipids. *J. Am. Chem. Soc.* **2003**, *125*, 5801–5810. [CrossRef] [PubMed]

66. Lee, J.; Bozzelli, J.W. Thermochemical and kinetic analysis of the allyl radical with O2 reaction system. *Proc. Combust. Inst.* **2005**, *30*, 1015–1022. [CrossRef]

67. El-Agamey, A.; McGarvey, D.J. First Direct Observation of Reversible Oxygen Addition to a Carotenoid-Derived Carbon-Centered Neutral Radical. *Org. Lett.* **2005**, *7*, 3957–3960. [CrossRef] [PubMed]
68. Wright, J.S.; Shadnia, H.; Chepelev, L.L. Stability of carbon-centered radicals: Effect of functional groups on the energetics of addition of molecular oxygen. *J. Comput. Chem.* **2009**, *30*, 1016–1026. [CrossRef] [PubMed]
69. Dibble, T.S.; Sha, Y.; Thornton, W.F.; Zhang, F. Cis–Trans Isomerization of Chemically Activated 1-Methylallyl Radical and Fate of the Resulting 2-Buten-1-peroxy Radical. *J. Phys. Chem. A* **2012**, *116*, 7603–7614. [CrossRef]